Investigation of octupole vibrational states in ¹⁵⁰Nd via inelastic proton scattering (*p*,*p'γ*)

M. Elvers,[1,2,*] S. Pascu,[1,3,†] T. Ahmed,[4] T. Ahn,[2] V. Anagnostatou,[2,5] N. Cooper,[2] C. Deng,[4] J. Endres,[1] P. Goddard,[2,5]
A. Heinz,[2,6] G. Ilie,[2,3] E. Jiang,[4] C. Küppersbusch,[1] D. Radeck,[1,2] D. Savran,[2,7,8] N. Shenkov,[4] V. Werner,[2] and A. Zilges[1]

[1]*Institut für Kernphysik, Universität zu Köln, DE-50937 Köln, Germany*
[2]*Wright Nuclear Structure Laboratory, Yale University, New Haven, Connecticut 06520-8120, USA*
[3]*National Institute for Physics and Nuclear Engineering, RO-77125 Bucharest-Magurele, Romania*
[4]*University of Richmond, Richmond, Virginia 23173, USA*
[5]*Department of Nuclear Physics, University of Surrey, Guildford GU2 7XH, United Kingdom.*
[6]*Fundamental Physics, Chalmers University of Technology, SE-412-916 Göteborg, Sweden*
[7]*ExtreMe Matter Institute EMMI and Research Division, GSI, Helmholtzzentrum, Darmstadt, Germany*
[8]*Frankfurt Institute for Advanced Studies FIAS, Frankfurt, Germany*

Octupole vibrational states were studied in the nucleus ¹⁵⁰Nd via inelastic proton scattering with 10.9-MeV protons, which are an excellent probe to excite natural parity states. For the first time in ¹⁵⁰Nd, both the scattered protons and the γ rays were detected in coincidence, giving the possibility to measure branching ratios in detail. Using the coincidence technique, the $B(E1)$ ratios of the decaying transitions for 10 octupole vibrational states and other negative-parity states to the yrast band were determined and compared to the Alaga rule. The positive and negative-parity states revealed by this experiment are compared with interacting boson approximation calculations performed in the $spdf$ boson space. The calculations are found to be in good agreement with the experimental data, for both positive and negative-parity states.

PACS number(s): 21.10.Re, 23.20.Lv, 21.10.Hw, 27.70.+q

I. INTRODUCTION

Octupole vibrations play a fundamental role in the description of low-lying negative-parity states. In a microscopic model, those states are described as a coherent superposition of 1-particle-1-hole excitations between an intruder state and a state of the same major shell with spin difference $\Delta l = \Delta j = 3$ [1]. Collective excitations in vibrational rare-earth nuclei, with both proton and neutron numbers in the proximity of a shell closure, are macroscopically described as (multi)phonon excitations [2]. Further away from shell closures, when prolate quadrupole deformation in the ground state is established, rotational bands are superimposed on the vibrations [3,4].

The nucleus ¹⁵⁰Nd ranks among the transitional nuclei between spherical harmonic vibrators and axially symmetric rotors [5]. Unlike a vibrator, this nucleus has a spheroidal shape and the quantum number K is rather well defined. Consequently, similar to perfect rotors, a band structure with β-, γ-, and an octupole-vibrational band exists in this nucleus [6]. However, the energy ratio, $E_{4_1^+}/E_{2_1^+} = 2.93$, is between a vibrator and a rotor. Furthermore, the relative transition strengths $\frac{B(E2:J^+ \to (J-2)^+)}{B(E2:2^+ \to 0^+)}$ of the yrast band members as a function of the angular momentum J lie between the predictions for an axially symmetric rotor and a vibrator.

While the level structure and decay properties of positive-parity states of even spin in the low-energy region are well established in this nucleus, the knowledge concerning low-energy negative-parity states is rather sparse. Up to now, only

the decay of the first two members of the $K^\pi = 0^-$ octupole band were observed and the energies of the $J^\pi = 1^-$ to $J^\pi = 7^-$ state were determined by means of inelastic particle scattering (p, p') [7]. Recently, those states were theoretically described by Bizzeti *et al.* using a model valid for nuclear shapes close to axial symmetry [8].

The goal of this experiment was to determine the ratios of the $B(E1)$ transitions strengths of the remaining two known members in this band and to determine the K quantum number of higher-lying negative-parity states. An approximate agreement with the Alaga rule [9] would further confirm the existence of a spheroidal shape.

The structure of ¹⁵⁰Nd was interpreted in terms of the first-order phase transition from spherical harmonic vibrator to axially deformed nuclei [5]. The observed agreement revealed that this nucleus is the best case so far of an empirical realization of the X(5) critical point symmetry [10]. However, the X(5) predictions are made only for the yrast and for the β-vibrational bands [or $s = 1$ and $s = 2$ bands in the X(5) description]. The model gives no predictions for the γ-vibrational band and, more important for the present discussion, for the octupole-vibrational states. Several attempts have been made to describe the negative-parity states for this type of nuclei; for example, the authors of Ref. [11] considered a collective Hamiltonian for the rotation-vibration motion in which the axial quadrupole and octupole degrees of freedom are coupled through the centrifugal interaction, or in Ref. [8] the collective motion was investigated based on a new parametrization of the octupole and quadrupole degrees of freedom. Another nucleus proposed to be an empirical realization of the X(5) critical point symmetry (¹⁵²Sm) has already been investigated using the interacting boson approximation (IBA)-$spdf$ model

approach and a good agreement with the experimental data was concluded [12]. In the present paper, we compare the new experimental results for ^{150}Nd with calculations performed in the framework of the IBA-$spdf$ model. The reproduction of the $E1$ transition rates is found to be in good agreement with the predictions given by the IBA calculations, especially for the $K^{\pi} = 0^{-}$ band.

The experimental setup and the data analysis are introduced in Secs. II and III, respectively. Thereafter, in Sec. IV, the results are discussed and compared to the theoretical calculations.

II. EXPERIMENTAL SETUP

A 1.5 mg/cm^2 thick and 98% enriched self-supporting ^{150}Nd target was bombarded with a 10.9- MeV proton beam provided by the ESTU Tandem Accelerator at the Wright Nuclear Structure Laboratory (WNSL) at Yale University. The experiment lasted for 120 h at an average beam current of 4 nA and an average coincidence rate of about 2 KHz $p\gamma$.

For the detection of the scattered protons, five silicon surface-barrier detectors were used, covering a solid angle of 5%. Three of them had a thickness of 1 mm, two had a thickness of 5 mm. The elastically scattered protons are completely stopped in both types of detectors. The setup was optimized for high efficiency by placing all detectors as close as possible to the target and it was kept flexible by allowing a positioning of the detectors in all three spatial directions. To achieve a high ratio of inelastically to elastically scattered protons, four detectors were placed at $\approx$130° backward angles where the cross section for elastically scattered protons is orders of magnitudes lower. Using a ^{228}Th α source, the energy resolution at 8.784 MeV was determined ranging from 55 to 90 KeV for the different detectors while the resolution degraded to values between 110 to 280 KeV in-beam owing to straggling effects in the target and increased electronic noise.

The γ rays were detected by the YRAST-Ball spectrometer [13], which is situated at WNSL providing up to 10 segmented high-purity germanium (HPGe) clover detectors. Each detector consists of four crystals with its own preamplified time and energy output. Each clover detector is surrounded by bismuth germanate (BGO) and actively shielded. The total photopeak efficiency of the array is on the order of 2% at 1332 KeV with an average energy resolution of 2 keV. In the present experiment, in total nine detectors were used; two were placed at 45° with respect to the beam axis, five at 90°, and two at 135°. The beam was stopped by a carbon-and-lead-shielded beam dump 2 m downstream which strongly reduced the neutron and γ-ray background. The data acquisition was done by three 16-channel analog-to-digital converters, three 16-channel time-to-digital converters (TDCs) and a logic unit based on versa module eurocard (VME) electronics. Data were acquired using three triggers: $p\gamma$ coincidences, downscaled single HPGe, and downscaled silicon events.

III. ANALYSIS

The single leaves of each clover were calibrated in energy and their relative efficiencies were determined using a ^{152}Eu
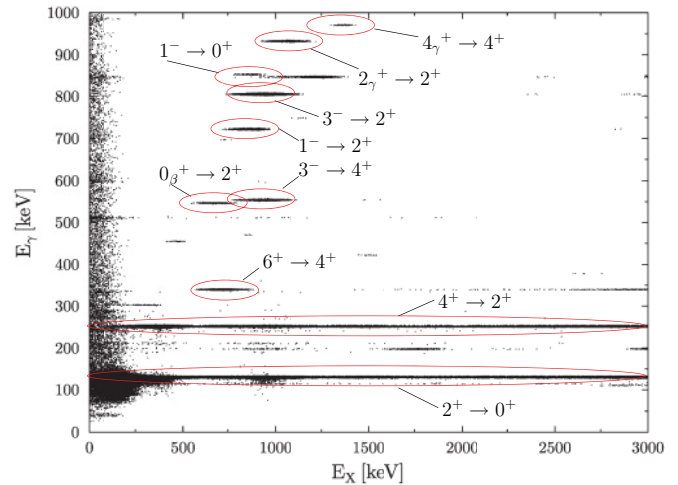

FIG. 1. (Color online) The $p\gamma$ matrix of ^{150}Nd. The transition energy E_{γ} is plotted versus the excitation energy E_X. Owing to the worse energy resolution in the silicon detectors in comparison to the HPGe detectors, transitions appear as narrow lines. This graphical representation of the $p\gamma$ matrix nicely shows the strength of the method to investigate the decay pattern of excited states.

source placed at target position. The silicon detectors were calibrated using peaks in the proton single spectra corresponding to elastic scattering and to excitations of the first excited states of ^{12}C, ^{16}O, and ^{150}Nd measured in the in-beam spectra. In a next step, the energy shift factors were determined and the prompt and random windows were applied to the time-difference spectra to reduce the background. To further reduce the Compton background in the lower energy part and to increase the photo-peak efficiency, the energies in the four leaves of a clover detector were added eventwise using an addback algorithm [14].

Using the sorting code CSCAN [15], the proton-γ-coincidence matrix ($p\gamma$ matrix), all single spectra, and the γ-γ-coincidence matrix ($\gamma\gamma$ matrix) were generated. An excerpt of the $p\gamma$ matrix is shown in Fig. 1. All transitions appear as narrow lines owing to the worse energy resolution of the silicon detectors in comparison to the good energy resolution of HPGe detectors. Both the $2^{+} \to 0^{+}$ and the $4^{+} \to 2^{+}$ transition cover the entire range of the excitation energies E_X giving rise to the fact that most of the states decay via those states to the ground state.

The necessity to detect both the scattered proton and the γ transition is illustrated in Fig. 2. Without coincidence condition, the γ-ray spectrum (a) shows the $e^{+}e^{-}$ annihilation line and the neutron edges as main contributions. In particular, no indication for transitions of states in ^{150}Nd are visible. However, when a gate with $750\,\text{keV} \leqslant E_X \leqslant 950$ KeV is applied in the proton spectrum, peaks corresponding to the decay of states in ^{150}Nd located at this excitation energy are clearly visible (c). Similarly, the particle spectrum is dominated by the elastic lines of ^{12}C, ^{16}O, and ^{150}Nd and their first excited states (b). If a gate is applied at a transition energy of the first $J^{\pi} = 1^{-}$ state in the γ-ray spectrum, a peak corresponding to the energy of the $J^{\pi} = 1^{-}$ state is

clearly visible in the silicon spectrum (d). The fluctuations at 10.5 MeV are the remnants of the elastic line of ^{150}Nd.

IV. RESULTS AND DISCUSSION

Using the $p\gamma$-coincidence matrix, the level scheme of ^{150}Nd was corrected and extended. In total, 37 levels up to 2 MeV were excited and 64 transitions were observed. In particular, the transitions of 8 states being previously excited in inelastic particle scattering experiments were found [7] and 12 new states were observed for the first time. Table I summarizes the results on ^{150}Nd obtained from the present experiment.

In the $K^{\pi} = 0^{-}$ band, the first four members (1^{-}, 3^{-}, 5^{-}, and 7^{-}) were excited and branching ratios of the latter two were determined for the first time. The experimental branching ratios and the predictions by the Alaga rule are listed in Table II, showing a good agreement for the first three states and an underprediction for the $J^{\pi} = 7^{-}$ state by the Alaga rule. The approximate agreement with the Alaga rule for the first three band members is another strong indication for an axially deformed rotor with a separable rotational motion. The transitions of higher-lying negative-parity states were observed for the first time. Similar to the states described above, most of the states have $K^{\pi} = 0^{-}$ character according to the Alaga rule, which is shown in Table II. Two states show a

significant branching to the 0^{+}_{β} vibrational band, giving rise to the assumption that these states have a large component of the β-vibrational in their wave function. The energies of those two candidates are located at 1545 and 1864 KeV, which is in the region of the sum energy $E_{\text{sum}} = E_{\text{oct,1}^-} + E_{\beta,2^+} = 1704$ KeV, as predicted in Ref. [3]. All corresponding states are marked with $\mathcal{O}_{\beta}$ in Table I.

The interacting boson model [16] provides a phenomenological approach for studying nuclear structure by introducing bosons of a given spin. Each type of boson is associated with a corresponding multipole mode. The quadrupole vibration and deformation are described in terms of s and d bosons ($L = 0$ and $L = 2$), while negative-parity states are described by introducing p and f bosons ($L = 1$ and $L = 3$). The f boson has been introduced to describe the octupole vibrational bands in quadrupole deformed nuclei [17–19]. The physical nature of the p boson is not yet very clear. In Ref. [20] it was assumed that the origin of the p boson could be a possible correction of the spurious center-of-mass motion of the quadrupole-octupole intrinsic system and in Ref. [21] the p boson was related to the giant dipole resonance. Despite these studies, the physical meaning of the p boson remains an open question.

Calculations were performed in the $spdf$ IBA-1 framework (no distinction was made between protons and neutrons) using the extended consistent Q formalism [22]. The Hamiltonian employed in the present paper is the natural extension of the

FIG. 2. Single and coincidence spectra of a silicon detector and a clover detector. The coincidence spectra were corrected for random coincidences. The single spectra are dominated by background reactions while the gated spectra clearly show the transitions within ^{150}Nd. A clover single spectrum (one leaf, 1 h run) and a single silicon spectrum (all runs) are shown in panels (a) and (b), respectively, while the gated spectra (all runs) are shown in panels (c) and (d).

TABLE I. States up to 2 MeV and their decay observed in the ^{150}Nd$(p, p'\gamma)$ experiment. Octupole states strongly decaying to the β-vibrational band are marked with $\mathcal{O}_\beta$. The state energy E, the initial and final spin and K quantum number $J_{i,f}^\pi$ $K_{i,f}^\pi$, the final energy E_f, the energy of the γ-ray E_γ and the branching ratios I_γ are listed.

E (keV)	K_i^π	J_i^π		J_f^π	K_f^π	E_f (keV)	E_γ (keV)	I_γ
130.21(8)	0_1^+	2^+	$\rightarrow$	0^+		0.00(0)	130.2	100.0
381.45(11)	0_1^+	4^+	$\rightarrow$	2^+	0_1^+	130.21(8)	251.24	100.0
675.37(17)	0_β^+	0^+	$\rightarrow$	2^+	0_1^+	130.21(8)	546.06	100.0
720.40(50)	0_1^+	6^+	$\rightarrow$	4^+	0_1^+	381.45(11)	339.70	100.0
850.79(21)	0_β^+	2^+	$\rightarrow$	4^+	0_1^+	381.45(11)	469.40	28.8(40)
				2^+	0_1^+	130.21(8)	720.61	100.0(130)
				0^+		0.00(0)	850.70	14.5(64)
853.06(21)	0^-	1^-	$\rightarrow$	2^+	0_1^+	130.21(8)	722.91	100.0(134)
				0^+		0.00(0)	853.01	97.7(165)
934.96(20)	0^-	3^-	$\rightarrow$	4^+	0_1^+	381.45(11)	553.52	36.3(39)
				2^+	0_1^+	130.21(8)	804.73	100.0(104)
1061.99(20)	2_γ^+	2^+	$\rightarrow$	4^+	0_1^+	381.45(11)	680.29	5.5(8)
				2^+	0_1^+	130.21(8)	931.78	100.0(106)
				0^+		0.00(0)	1061.98	80.4(88)
1129.57(21)	0^-	5^-	$\rightarrow$	6^+	0_1^+	720.40(50)	409.23[a]	24.3(37)
				4^+	0_1^+	381.45(11)	748.07[a]	100.0(118)
1129.70(110)	0_1^+	8^+	$\rightarrow$	6^+	0_1^+	720.40(50)	409.50[c]	100.0
1137.59(41)	0_β^+	4^+	$\rightarrow$	6^+	0_1^+	720.40(50)	416.94[a]	43.5(76)
				4^+	0_1^+	381.45(11)	756.40[a]	100.0(143)
1183.33(21)		$\leqslant 2$	$\rightarrow$	3^-	0^-	934.96(20)	248.34[a]	100.0(142)
				1^-	0^-	853.06(21)	330.30	66.1(102)
1200.49(27)		$3(^-)$	$\rightarrow$	4^+	0_1^+	381.45(11)	819.16	22.4(37)
				2^+	0_1^+	130.21(8)	1070.15	100.0(118)
1284.59(20)		1^-	$\rightarrow$	3^-	0^-	934.96(20)	349.63	67.8(103)
				1^-	0^-	853.06(21)	430.88	100.0(132)
				2^+	0_β^+	850.79(21)	434.09	9.8(36)
1351.57(21)[b]	2_γ^+	4^+	$\rightarrow$	2^+	2_γ^+	1061.99(20)	289.57[a]	6.4(10)
				4^+	0_1^+	381.45(11)	970.07[a]	100.0(112)
				2^+	0_1^+	130.21(8)	1221.42[a]	38.7(49)
1432.94(24)	0^-	(7^-)	$\rightarrow$	8^+	0_1^+	1129.70(110)	303.33[a]	49.6(137)
				6^+	0_1^+	720.40(50)	712.44	100.0(223)
1435.90(20)		4^+	$\rightarrow$	$3(^-)$		1200.49(27)	234.41	100.0
				2^+	2_γ^+	1061.99(20)	373.91	100.0
1483.67(21)[b]		3^-	$\rightarrow$	$3(^-)$		1200.49(27)	283.00[a]	31.7(44)
				2^+	2_γ^+	1061.99(20)	421.71[a]	33.7(44)
				4^+	0_1^+	381.45(11)	1102.14[a]	100.0(120)
				2^+	0_1^+	130.21(8)	1353.52[a]	85.9(113)
1488.52(20)[a]		4, (0, 2)	$\rightarrow$	1^-		1284.59(20)	204.15[a]	31.4(74)
				2^+	0_1^+	130.21(8)	1358.31[a]	100.0(159)
1489.29(20)[a]		0, 1, 2	$\rightarrow$	0^+	0_β^+	675.37(17)	813.92[a]	100.0
1496.75(20)[a]		3, (2, 4, 5)	$\rightarrow$	4^+	0_β^+	1137.59(41)	359.16[a]	100.0
1517.67(22)[a]		4, 5, 6	$\rightarrow$	6^+	0_1^+	720.40(50)	797.21[a]	69.4(145)
				4^+	0_1^+	381.45(11)	1136.29[a]	100.0(160)
1545.06(36)[b]	$\mathcal{O}_\beta$	3^-	$\rightarrow$	2^+	0_β^+	850.79(21)	694.05[a]	25.0(71)
				2^+	0_1^+	130.21(8)	1415.06[a]	100.0(149)
1580.10(30)[b]		3^-	$\rightarrow$	4^+	0_1^+	381.45(11)	1198.50[a]	100.0(121)
				2^+	0_1^+	130.21(8)	1450.05[a]	67.5(93)
1645.34(26)[a]		5, (4)	$\rightarrow$	6^+	0_1^+	720.40(50)	924.82[a]	57.0(93)
				4^+	0_1^+	381.45(11)	1264.01[a]	100.0(138)
1645.97(26)[a]		3, 5, (2, 4)	$\rightarrow$	4^+	2_γ^+	1351.57(21)	294.29[a]	100.0(159)
				4^+	0_β^+	1137.59(41)	508.50[a]	34.5(88)
1648.66(20)[a]		1, (0, 2)	$\rightarrow$	2^+	0_1^+	130.21(8)	1518.45[a]	100.0
1738.86(20)		0^+	$\rightarrow$	2^+	0_1^+	130.21(8)	1608.65	100.0
1765.28(22)[a]		0, 1, 2, 3	$\rightarrow$	1^-	0^-	853.06(21)	912.16[a]	100.0(140)
				1^-		1284.59(20)	480.75[a]	42.1(90)

TABLE I. (*Continued*)

E (keV)	K_i^π	J_i^π		J_f^π	K_f^π	E_f (keV)	E_γ (keV)	I_γ
1777.08(20)[a]		1, 2, 3, 4, 5	$\rightarrow$	3^-		1580.10(30)	196.98[a]	100.0(0)
1782.21(20)[b]		(4^+)	$\rightarrow$	3^-	0^-	934.96(20)	847.25[a]	100.0(0)
1799.91(20)[b]		(5^-)	$\rightarrow$	3^-	0^-	934.96(20)	864.22[a]	100.0(190)
				6^+	0_1^+	720.40(50)	1080.23[a]	15.2(74)
1864.20(20)[b]	$\mathcal{O}_\beta$	3^-	$\rightarrow$	2^+	0_β^+	850.79(21)	1014.08[a]	100.0(126)
				4^+	0_1^+	381.45(11)	1482.75[a]	80.7(112)
1906.52(20)[b]		4^+	$\rightarrow$	2^+	2_γ^+	1061.99(20)	844.53[a]	100.0(0)
1909.34(20)[a]		0, 1, 2, 3, 4	$\rightarrow$	2^+	0_1^+	130.21(8)	1779.13[a]	100.0(0)
1975.62(20)[a]		1, 2, 3, 4, 5	$\rightarrow$	$3^{(-)}$		1200.49(27)	775.13[a]	100.0(0)
1984.94(20)[a]		1, 2, 3, 4, 5	$\rightarrow$	3^-	0^-	934.96(20)	1049.98[a]	100.0(0)

[a]observed for the first time, not in NNDC.
[b]state without transitions observed in inelastic particle scattering.
[c]Not excited, taken from NNDC.

$\hat{H}_{sd}$ Hamiltonian and is able to describe simultaneously the positive- and negative-parity states:

$$
\hat{H}_{spdf} = \epsilon_d \hat{n}_d + \epsilon_p \hat{n}_p + \epsilon_f \hat{n}_f + \kappa (\hat{Q}_{spdf} \cdot \hat{Q}_{spdf})^{(0)}
$$
$$
+ \text{a}_3 [(\hat{d}^\dagger \tilde{d})^{(3)} \cdot (\hat{d}^\dagger \tilde{d})^{(3)}]^{(0)} + \text{a}_4 [(\hat{d}^\dagger \tilde{d})^{(4)} \cdot (\hat{d}^\dagger \tilde{d})^{(4)}]^{(0)},
$$
(1)

where ϵ_d, ϵ_p, and ϵ_f are the boson energies and $\hat{n}_p$, $\hat{n}_d$, and $\hat{n}_f$ are the boson number operators. In the $spdf$ model, the quadrupole operator is considered as being [23]

$$
\hat{Q}_{spdf} = \hat{Q}_{sd} + \hat{Q}_{pf} = \left[(\hat{s}^\dagger \tilde{d} + \hat{d}^\dagger \hat{s})^{(2)} - \frac{\sqrt{7}}{2} (\hat{d}^\dagger \tilde{d})^{(2)} \right]
$$
$$
- \frac{3\sqrt{7}}{5} [(p^\dagger \tilde{f} + f^\dagger \tilde{p})]^{(2)} + \frac{9\sqrt{3}}{10} (p^\dagger \tilde{p})^{(2)}
$$
$$
+ \frac{3\sqrt{42}}{10} (f^\dagger \tilde{f})^{(2)}.
$$
(2)

The quadrupole electromagnetic transition operator is

$$
\hat{T}(E2) = e_2 \hat{Q}_{spdf},
$$
(3)

where e_2 represents the boson effective charge.

This form of the quadrupole operator implies using the same quadrupole parameter strength κ to describe sd bosons and pf bosons. In addition, the rotational SU$_{spdf}$(3) structure is also generated by this form [Eq. (2)] of the $\hat{Q}_{spdf}$ quadrupole operator [23]. In this way no additional free parameters are used in the calculations. The structure of both the positive- and the negative-parity states is also described by the same parameter-free quadrupole operator $\hat{Q}_{spdf}$. The only degree of freedom in describing the negative-parity states lies in the p and f vibrational energies ϵ_p and ϵ_f. However, these are defined largely by the experimental locations of the lowest 1^- and 3^- states.

For the $E1$ transitions there is more than one operator in the $spdf$ algebra. Consequently, a linear combination of the three allowed one-body interactions was taken:

$$
\hat{T}(E1) = e_1 \big[\chi_{sp}^{(1)} (s^\dagger \tilde{p} + p^\dagger \tilde{s})^{(1)} + (p^\dagger \tilde{d} + d^\dagger \tilde{p})^{(1)}
$$
$$
+ \chi_{df}^{(1)} (d^\dagger \tilde{f} + f^\dagger \tilde{d})^{(1)} \big],
$$
(4)

where e_1 is the effective charge for the $E1$ transitions and $\chi_{sp}^{(1)}$ and $\chi_{df}^{(1)}$ are two model parameters.

TABLE II. $B(E1)$ ratios $R_{\exp} = \frac{B(E1; J_i^- \rightarrow (J_i+1)^\pi)}{B(E1; J_i^- \rightarrow (J_i-1)^\pi)}$ to the yrast band of octupole-vibrational states and negative-parity states compared with IBA-$spdf$ calculations and with the Alaga-rule predictions. Furthermore, the experimental energy $E_{\exp}$, the initial spin J_i^π, the final K quantum number K_f^π, and the IBA calculations for the energy and branching ratio $E_{\text{IBA-}spdf}$ (keV) and $R_{\text{IBA-}spdf}$ are given. Most of the states are in good agreement with the IBA calculations but differ considerably from the Alaga rule predictions. Members of the $K^\pi = 0^-$ band are marked in bold font.

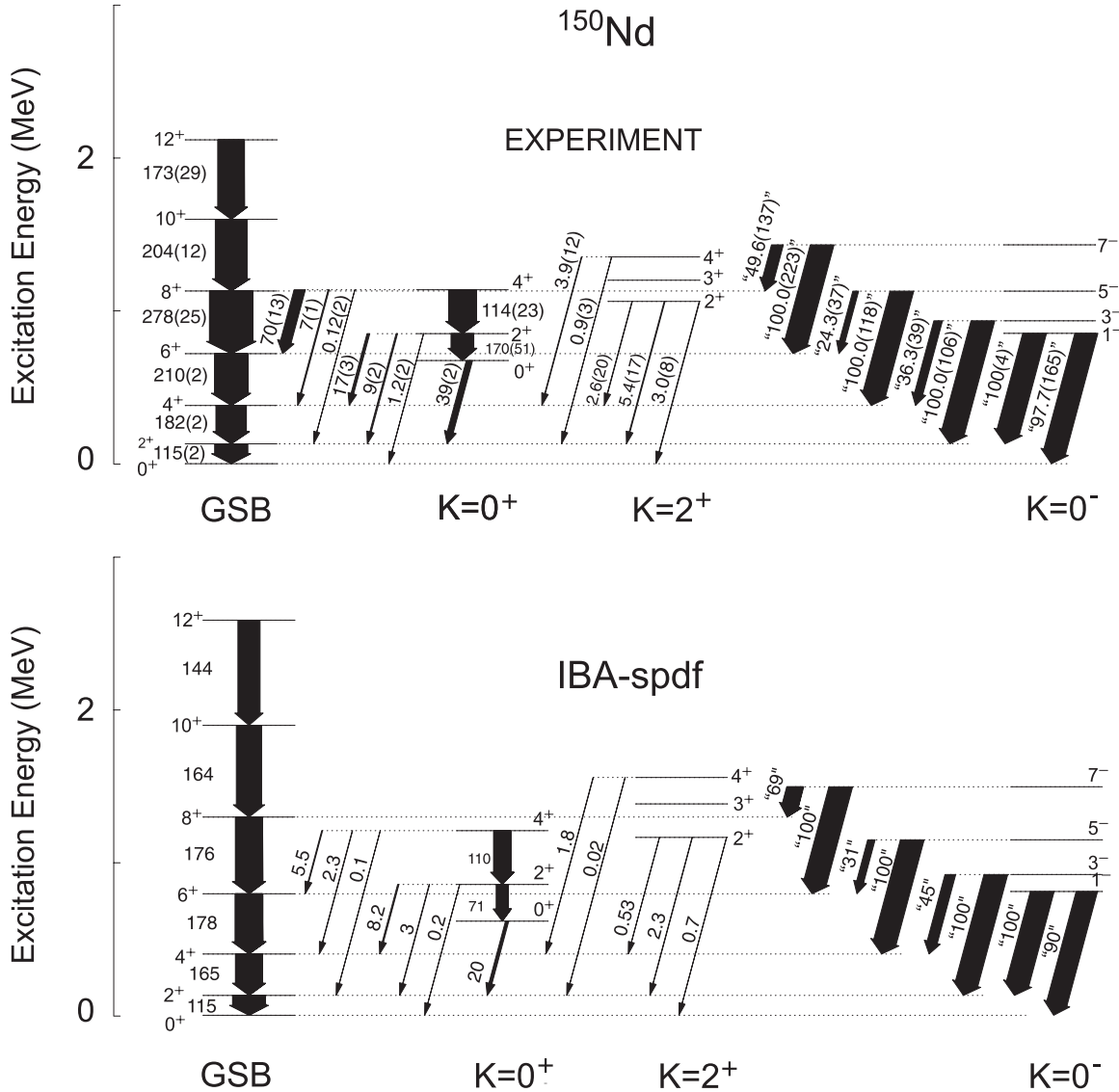| $E_{\exp}$ (keV)	J_i^π	K_f^π	$R_{\exp}$	$E_{\text{IBA-}spdf}$ (keV)	$R_{\text{IBA-}spdf}$	Alaga rule $K^\pi = 0^-$	$K^\pi = 1^-$
853.1	1^-	0_1^+	1.68(36)	810.1	1.82	2.00	0.50
935.0	3^-	0_1^+	1.12(17)	921.2	1.38	1.33	0.75
1129.6	5^-	0_1^+	1.48(29)	1148.0	1.89	1.20	0.83
1432.9	7^-	0_1^+	6.43(228)	1494.8	4.2	1.14	0.88
1483.7	3^-	0_1^+	2.16(38)	1414.7	1.77	1.33	0.75
1517.7	4,5,6	0_1^+	2.01(53)	1517.7	1.1	1.20	0.83
1580.1	3^-	0_1^+	2.62(48)	1694.5	2.17	1.33	0.75
1645.3	4,5,6	0_1^+	1.46(31)	1986.8	1.15	1.20	0.83

FIG. 3. Comparison between experimental (top) and calculated (bottom) excitation energies and transition probabilities or relative intensities of the γ-ray transitions for the low-lying levels in ^{150}Nd. The known $B(E2)$ values are indicated for the positive-parity states. The numbers in quotation marks are the relative values (branching ratios) and are indicated for the negative-parity states. The experimental information is taken from Refs. [5,25,26] and from the present work. The bands are labeled according to their K quantum number.

The calculations were performed using the computer code OCTUPOLE [24]. The Hamiltonian is diagonalized in a Hilbert space with a total number of bosons $N_B = n_s + n_d + n_p + n_f$. For the present calculations we used an extended basis allowing up to three negative-parity bosons ($n_p + n_f = 3$). The vibrational strengths used in the calculations are $\epsilon_d = 0.53$ MeV, $\epsilon_p = 1.32$ MeV, and $\epsilon_f = 1.12$ MeV while the quadrupole-quadrupole interaction strength has a value of $\kappa = -18.5$ keV. The other two terms introduced in the Hamiltonian (the octupole and the hexadecapole terms) are included only to obtain a better reproduction for the relative inter- and intraband transitional rates. The strengths of these two terms are set to values of $a_3 = 0.04$ MeV and $a_4 = 0.10$ MeV, respectively.

The quality of the present calculation in describing the experimental data can be seen in Fig. 3. The numbers on the transition arrows represent the absolute $B(E2)$ values given in Weisskopf Units (W.u.) and are indicated for the positive-parity states, and relative intensities of the γ-ray transitions (branching ratios) are given for the negative-parity states (only the lifetime of the 1^- state is measured [25]; hence, only one absolute $B(E1)$ value is known). The overall agreement between the experimental and calculated energies is good. The spacing of the states is reasonably well reproduced by the calculations for all the bands involved in our analysis (the ground-state band, the β- and γ-vibrational bands, and the $K^\pi = 0^-$ octupole vibrational band). The first excited 0^+ state is located less than 50 keV below the experimental

one with an energy of 675.4 keV [26]. The location of this state is considered a key prediction in the X(5) model because the ratio $E(0_2^+)/E(2_1^+)$ is fixed at a value of 5.67 [27] (cannot be fitted to obtain a better agreement) and gives an important fingerprint for the presence of the first-order critical point symmetry. The relative values of the $E1$ and $E2$ transition probabilities are in very good agreement with the experiment, as can be seen in Fig. 3 for the negative-parity states (only $E1$ transitions). However, the absolute $B(E2)$ values are, in general, underestimated by a factor that usually does not exceed a value of two. Especially for the higher spin states, the finite boson number effect plays an important role in lowering the predictions for $E2$ transition strengths. This behavior was already observed in Ref. [28], where a detailed comparison between X(5) critical point symmetry and the IBA model predictions for this region was made.

For the $E2$ transitions we obtained the agreement from Fig. 3 by using a value of $e_2 = 0.13$ e b for the effective charge. For the $E1$ transitions values of $\chi_{sp} = -1.31$ and $\chi_{df} = 0.77$ were used in the fit to account for the observed $E1$ transition rates. The effective charge is not taken into consideration in the present calculations because only the lifetime of the first 1^- state is measured and the extracted $E1$ absolute strength can only be used for normalization. For the moment no other absolute $E1$ strengths are experimentally known for the negative-parity states and no comparison with the calculated values can be made. Our discussion is based only on the relative values obtained in the present experiment. A comparison between the experimental $B(E1)$ ratios with the calculated ones is given in Table II. In addition, the predictions of the Alaga rule are given for $K^\pi = 0^-$ and for $K^\pi = 1^-$ bands. For the $K^\pi = 0^-$ band the agreement of the IBA calculations with the experiment is remarkably good, both for the energies and for the relative transition probabilities. Most of the IBA predictions are within the experimental uncertainties or very close to these values. The predictions of the Alaga rule are in good agreement with the experiment for the first three states ($J^\pi = 1^-$, 3^-, and 5^-) and show an underprediction for the last level ($J^\pi = 7^-$) of the $K^\pi = 0^-$ band. For the states belonging to higher K^π some additional assumptions about the spin parity of the states had to be made. Namely, we assumed that the levels at 1517.7 and 1645.3 keV have a $J^\pi = 5^-$ spin assignment. Also, a state located at 1200 keV was identified as the $J^\pi = 3^+$ member of the γ-vibrational band in an $(n, n'\gamma)$ experiment [29], while it was assigned as a $J^\pi = 3^\pm$ doublet within the scope of a $(d, d'\gamma)$ experiment [30]. Considering this ambiguity, this level was considered as having a positive parity in the present discussion, although only the energy of this level is given in the comparison presented in Fig. 3. For the other states in Table II the experimental data are very well described by the IBA calculations, while underestimated, in general, by the Alaga rule predictions. Additional calculations are needed to gain a deeper understanding from a microscopic point of view of the electric dipole transitions.

V. SUMMARY AND CONCLUSIONS

Within the scope of this work, the nucleus ^{150}Nd was investigated by means of a $(p, p'\gamma)$ experiment for the first time and 17 negative-parity states were observed. In particular, the branchings of the first four members for the $K^\pi = 0^-$ octupole band were observed. Most of the remaining negative-parity states had $K^\pi = 0^-$ character and dominantly spins with $J = 3$ and 5 were excited. Three of those states show strong transitions to the β-vibrational band and can be explained by a strong mixing with states of the latter band. It is an open question if these states exist owing to the inner structure of ^{150}Nd or if the reaction mechanism is sensitive to states of this nature.

The structure of ^{150}Nd was discussed in terms of the IBA-*spdf* model. The energy levels and $E1$ and $E2$ transition probabilities are reasonably well described by the calculations. The relative values are in very good agreement with the experiment, although the absolute $B(E2)$ values are, in general, underestimated by the calculations. Especially for the higher spin states, the finite boson number effect plays an important role in lowering the predictions. The $E1$ transition probabilities are also well reproduced by the calculations, especially for the $K^\pi = 0^-$ band.

VI. OUTLOOK

Until the present day, in 15 rare-earth nuclei branching ratios of the band heads of both the $K^\pi = 0^-$ and the $K^\pi = 1^-$ band were observed, which, however, is insufficient for detailed systematics. Thus, $(p, p'\gamma)$ experiments are essential to provide the missing information and help to understand the inner structure of the remaining nuclei. For this reason, the design and development of a new silicon detector chamber started at the end of 2010 at Universität zu Köln. It will be included in the HORUS spectrometer in Cologne and will provide eight silicon detectors with a total efficiency of 5%. The distances between the detectors and the target are adjustable providing the possibility to run all silicon detectors at a maximum rate. Furthermore, $\Delta E - E$ measurements will be possible, giving the opportunity to perform additional inelastic scattering experiments, for example, $(d, d'\gamma)$ and $(p, t\gamma)$ reactions. The new setup will allow measurements which will trigger new theoretical studies of octupole related structures.

[1] P. A. Butler and W. Nazarewicz, Rev. Mod. Phys. **68**, 349 (1996).

[2] M. Wilhelm, E. Radermacher, A. Zilges, and P. von Brentano, Phys. Rev. C **54**, 449(R) (1996).

[3] W. Donner and W. Greiner, Z. Phys. **197**, 440 (1966).

[4] K. Neergård and P. Vogel, Nucl. Phys. A **145**, 33 (1970).

[5] R. Krücken *et al.*, Phys. Rev. Lett. **88**, 232501 (2002).

[6] H. H. Pitz *et al.*, Nucl. Phys. A **509**, 587 (1990).

[7] M. Pignanelli *et al.*, Nucl. Phys. A **559**, 1 (1993).

[8] P. G. Bizzeti and A. M. Bizzeti-Sona, Phys. Rev. C **81**, 034320 (2010).

[9] G. Alaga, K. Alder, A. Bohr, and B. R. Mottelson, K. Dan. Vidensk. Selesk. Mat. Fys. Medd. **29**, 1 (1955).

[10] F. Iachello, Phys. Rev. Lett. **87**, 052502 (2001).

[11] N. Minkov, P. Yotov, S. Drenska, W. Scheid, D. Bonatsos, D. Lenis, and D. Petrellis, Phys. Rev. C **73**, 044315 (2006).

[12] M. Babilon, N. V. Zamfir, D. Kusnezov, E. A. McCutchan, and A. Zilges, Phys. Rev. C **72**, 064302 (2005).

[13] C. W. Beausang *et al.*, Nucl. Instrum. Methods Phys. Res., Sect. A **452**, 431 (2000).

[14] P. K. Joshi, H. C. Jain, A. S. Medhi, S. Chattopadhyay, S. Bhattacharya, and A. Goswami, Nucl. Instrum. Methods Phys. Res., Sect. A **399**, 51 (1997).

[15] M. A. Caprio, J. J. Ressler, and H. Ai, program CSCAN (unpublished, 2004).

[16] A. Arima and F. Iachello, Phys. Rev. Lett. **35**, 1069 (1975).

[17] A. F. Barfield, B. R. Barrett, J. L. Wood, and O. Scholten, Ann. Phys. **182**, 344 (1988).

[18] P. D. Cottle and N. V. Zamfir, Phys. Rev. C **54**, 176 (1996).

[19] P. D. Cottle and N. V. Zamfir, Phys. Rev. C **58**, 1500 (1998).

[20] J. Engel and F. Iachello, Phys. Rev. Lett. **54**, 1126 (1985).

[21] M. Sugita, T. Otsuka, and P. von Brentano, Phys. Lett. B **389**, 642 (1996).

[22] R. F. Casten and D. D. Warner, Rev. Mod. Phys. **60**, 389 (1988).

[23] D. Kusnezov, J. Phys. A: Math. Gen. **23**, 5673 (1990).

[24] D. Kusnezov, computer code OCTUPOLE (unpublished).

[25] M. Zielińska, Int. J. Mod. Phys. E **13**, 71 (2004).

[26] E. Dermateosian and J. K. Tuli, Nucl. Data Sheets **75**, 827 (1995).

[27] R. F. Casten, Nat. Phys. **2**, 811 (2006).

[28] E. A. McCutchan, N. V. Zamfir, and R. F. Casten, Phys. Rev. C **71**, 034309 (2005).

[29] S. N. Tripathi, M. C. Schell, D. F. Coope, and M. T. McEllistrem, Bull. Am. Phys. Soc. **22**, 614, HG4 (1977).

[30] R. Katajanheimo, A. Siivola, and R. Lauhakangas, Z. Phys. A **297**, 123 (1980).